ISSN: 3067-929X
Research Article

Journal of Electronics Science and Electrical Research

Validation of Transfer Matrix Method Simulations with Experiment

Maria Masood*

Germany

***Corresponding author:** Maria Masood, Germany.

Submitted: 21 May 2025 **Accepted:** 24 May 2025 **Published:** 31 May 2025

https://doi.org/10.63620/MKJESER.2025.

Citation: *Masood, M. (2025). Validation of Transfer Matrix Method Simulations with Experiment. J of Electron Sci and Electrical Res, 2(2), 01-11.*

Abstract

This chapter validates the accuracy of Transfer Matrix Method (TMM) simulations for designing multilayer thin films by comparing them with experimental measurements. Five multilayer wafers were fabricated via the plasma-enhanced chemical vapour deposition (PECVD) method and sputtering techniques with various materials, including aluminum, silica and titanium nitride (TiN). The fabricated wafers were subjected to extensive testing via ellipsometry and scanning electron microscopy to measure the layer thickness, refractive indices, and optical properties. The experimental results closely match those of the TMM simulations, confirming the reliability of this design approach. Wafers with various multilayer configurations, including metal–insulator–metal (MIM) stacks, have demonstrated controlled absorption characteristics tailored to specific optical requirements. This study supports the use of TMMs for designing multilayer stacks for advanced optical applications, such as selective emitters in thermophotovoltaic systems, validating the approach for further development in optimizing multilayer designs.

Keywords: Transfer Matrix Method, Metal-Insulator-Metal, Multilayers, Simulations

Introduction

When a thin layer is deposited on a substrate, it is known as a thin film. For example, a reflective metal layer is deposited at the back of a glass substrate to make a mirror. When multiple layers of different or similar materials and thicknesses are deposited on a substrate, it becomes a multilayer stack that has an enormously broad range of applications [1-3]. Multilayer stacks are used to make structures with desired optical, thermal or electrical properties [4].

In this research, the thickness and refractive index of each layer were carefully considered and varied to obtain a stack that works as desired. It was important to test our design process for the absorption of the wafers via TMM simulations; in that context, a group of different multilayer stacks were fabricated in a cleanroom and extensively tested, and their optical properties were measured, studied and compared to quantify the soundness of the simulations.

There are a number of ways to fabricate multilayers as thin as a few nanometers up to micrometers [5, 6]. The multilayers in the devices studied in this work were built via the plasma- enhanced chemical vapour deposition (PECVD) method to deposit the dielectrics and sputtering to deposit the metals [7-11].

The PECVD technique is most popularly used in photovoltaics for making solar cells [12]. With this technique, large surface areas and a high degree of control of the properties of the thin films being deposited can be achieved by tuning the plasma.

In the sputtering technique, atoms from the surface of a target are ejected by high bombardment of ions or electrons and allowed to settle on a substrate (usually silicon). The ions in the plasma should have a minimum energy corresponding to the binding energy of the target atoms but are not very high because the ions penetrate deep inside the target, and the surface atoms are then not affected or ejected.

Description of the Wafers

Five multilayer thin films were studied on a silicon substrate. These multilayer wafers were made from CMOS-compatible materials [13-15] i.e., aluminum (Al), silica and titanium nitride (TiN). Wafers 1 and 2 were metal insulator metal (MIM) and metal insulator metal (MIMIM) stacks designed with Al and silica. These two wafers were intended for use as a selective emitter for a thermophotovoltaic system designed to peak around the bandgap wavelength of gallium arsenide (GaAs) [16-18]. The other wafers with TiN and silica multilayers (Wafer 3 and 4) were designed with the purpose of validating the simulations with experiments. The TiN layer on the silicon substrate (Wafer 5) was a test wafer designed to check the accuracy of the fabrication methods.

The specifications of these wafers are listed in Table 1.

Table 1: Five wafers of five different multilayer stacks.

	Insulator	Metal	Insulator	Metal	Insulator	Metal	Substrate
Wafer 1	120 nm Silica	-	-	50 nm Al	100 nm Silica	150 nm Al	Silicon
Wafer 2	120 nm Silica	50 nm Al	100 nm Silica	100 nm Al	100 nm Silica	150 nm Al	Silicon
Wafer 3	90 nm Silica	-	-	60 nm TiN	70 nm Silica	60 nm TiN	Silicon
Wafer 4	90 nm Silica	50 nm TiN	300 nm Silica	50 nm TiN	300 nm Silica	50 nm TiN	Silicon
Wafer 5	-	-	-	-	-	80 nm TiN	Silicon

The scanning electron microscopy (SEM) images of the fabricated Wafer 1 and Wafer 2 products described in Table 1 are shown in Figure 1 and Figure 2.

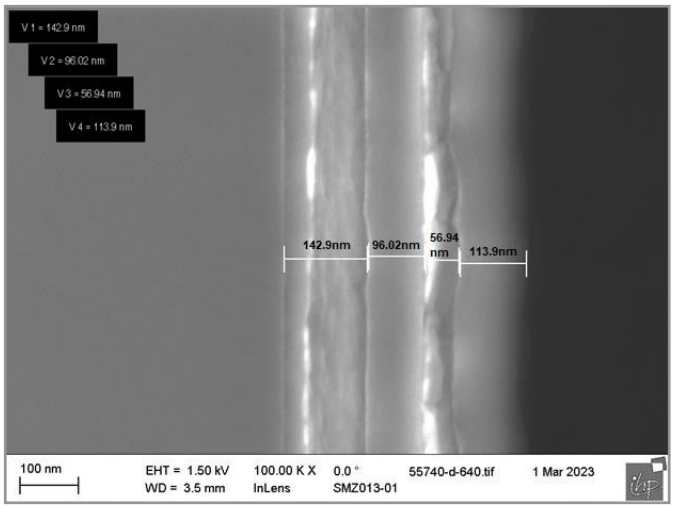

Figure 1: SEM images of the fabricated multilayer stack of Wafer 1 with the measured thickness of each layer. V1 is the bottom metallic layer of aluminum, followed by V2, V3 and V4 being the top layers.

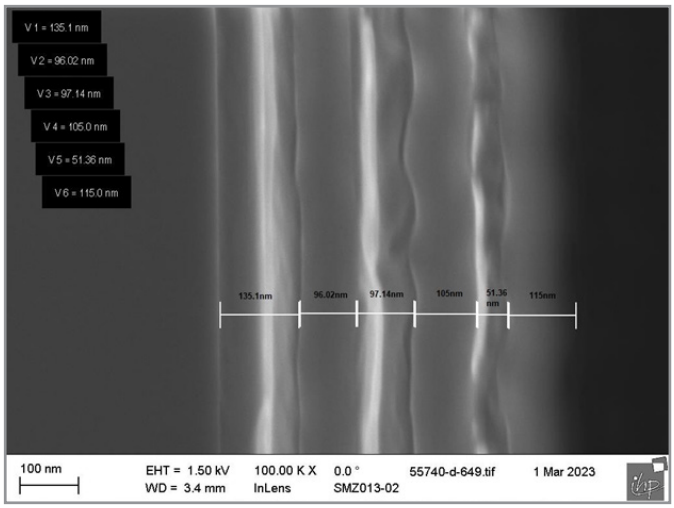

Figure 2: SEM images of the fabricated multilayer stack of Wafer 2 with the measured thickness of each layer. V1 is the bottom metallic layer of aluminum, followed by V2, V3, V4, V5 and V6 as the top layers.

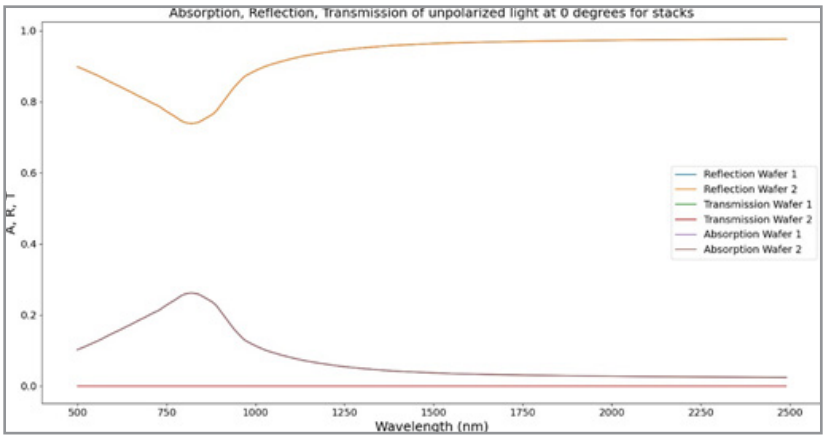

Figure 3: Absorption, reflection and transmission of Wafer 1 and Wafer 2 calculated via TMM simulations. The absorption peak around the bandgap wavelength of a GaAs converter cell was optimized.

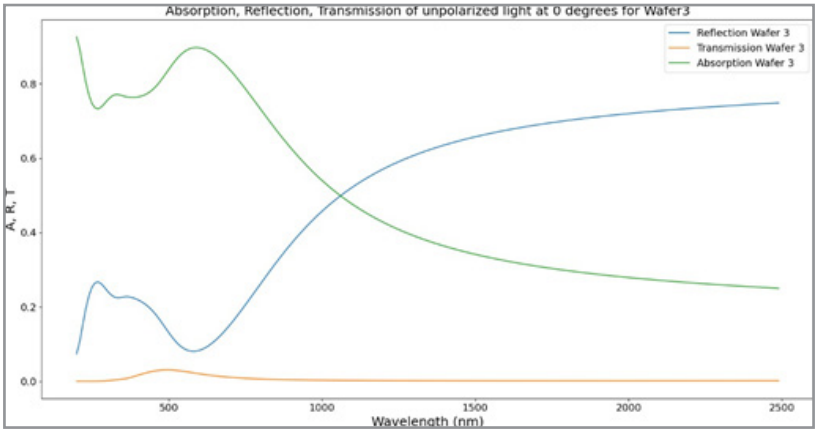

Figure 4: Absorption, reflection and transmission of Wafer 3 with TiN and silica multilayers calculated via TMM simulations.

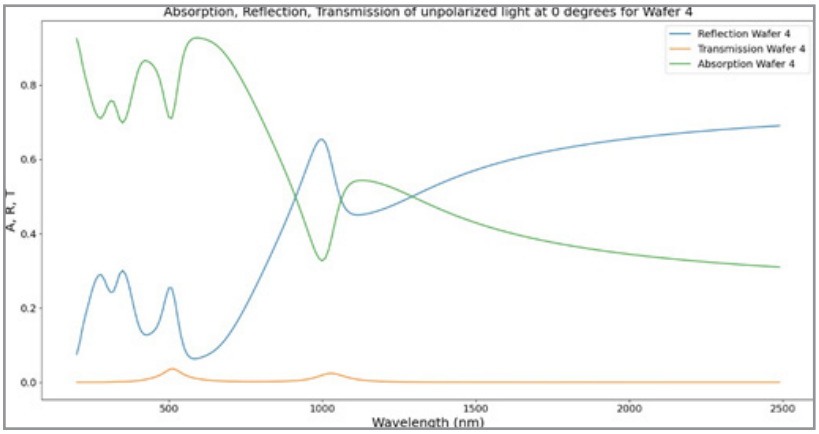

Figure 5: Absorption, reflection and transmission of Wafer 4 with TiN and silica multilayers calculated via TMM simulations.

The response of Wafer 1 and Wafer 2 is similar and has a peak in absorption around the bandgap wavelength of GaAs (870 nm), which was our reference converter cell. The response is similar because almost all the absorption takes place in the top MIM Fabry–Perot cavity. A Fabry–Perot cavity is well explained in [19]. The absorption peak due to the Fabry–Perot resonance in the bottom Fabry–Perot cavity is suppressed by the use of very thick metal layers; hence, the transmission into this bottom Fabry–Perot cavity is greatly reduced; therefore, the Fabry–Perot resonance in this cavity becomes weaker, resulting in a reduced absorption intensity. The intensity of the absorption peak is also similar because both wafers have the same thicknesses in the top cavity and are made of the same metal. Notably, the transmission of the whole stack is zero because of the 150 nm thick bottom Al metal layer, which prevents transmission.

The response of Wafer 3 and Wafer 4 is much greater when the TiN/silica multilayers are used, but these do not have a sudden drop in intensity, as would be required in the case of a selective emitter. Therefore, these methods have been used to study other parameters of multilayers, such as the refractive index, thickness of fabrication, ellipsometry parameters, etc.

Wafer 5 is a test wafer of a very thin TiN layer on a silicon substrate, and the desired thickness during fabrication in the clean room was between 50 nm and 100 nm. After the thickness was studied via ellipsometry, it was found to be approximately 80 nm in thickness.

Results

Verification of the Thickness of the Layers in the Wafers

After fabrication, and before dicing the wafer into smaller samples, the thickness of each layer at 9 different points in the wafer was measured via ellipsometry. Only the thicknesses of the top two layers of Wafer 1 and Wafer 2 were obtained via ellipsometry because it is difficult for the light to penetrate below the first Al layer; hence, the thicknesses below the Al layer were not obtained.

The penetration depth of light, δ, inside a metal layer is

$$\delta = \frac{\lambda}{2.\pi.k}$$

Equation 1

where

k is the absorption coefficient of the metal.

Λ is the wavelength of incident light As an example, the penetration depth of light calculated at 1000 nm for Al was approxi-

mately 17 nm, and that of TiN was approximately 44 nm. Since the penetration depth of light in the Al layer is low, light cannot penetrate beyond the first player to reach the other deeper layers. However, this is not the case for Wafer 3 and Wafer 4, since, in general, the TiN layers can be thicker than the Al layers.

Wafer 1 and Wafer 2:
These are noted in the Table 2 below. Here, layer 1 refers to the top insulator layer in the wafer.

As shown in Table 2 from the ellipsometry results, the fabricated insulator layer on the top is approximately 12 nm thicker than expected, and the Al layer was fixed in the model at a thickness of exactly 50 nm at all 9 points in the wafer. However, from the SEM images of both Wafer 1 and Wafer 2, the measured thickness is slightly less than the designed 120 nm top layer, and the second layer from the top is more or less similar to the designed thickness of 50 nm.

Table 2: Calculated thicknesses of the top two layers of Wafer1 and Wafer2 via ellipsometry.

9 points	Layer 1 in nm	Layer 2 in nm
Point 1	132.8207	50
Point 2	133.2997	50
Point 3	135.6206	50
Point 4	136.1073	50
Point 5	135.6932	50
Point 6	130.4108	50
Point 7	132.9804	50
Point 8	134.8564	50
Point 9	134.2519	50

Wafer 3: As shown in Table 3, for Wafer 3, the top insulator layer (Layer 1) thickness is slightly different at different points on the wafer but around the designed thickness. For layer 2, the Al layer thickness is slightly greater than the designed thickness but is only 4–6 nm thick, which should not affect the response much. Layers 3 and 4 are close to the designed thicknesses and do not vary much over different points on the wafer—Layer 4 of TiN is fixed in the model at exactly 60 nm, as designed.

Table 3: Calculated thicknesses of the different layers of Wafer3 via ellipsometry.

9 Points	Layer 1 (in nm)	Layer 2 (in nm)	Layer 3 (in nm)	Layer 4 (in nm)
Point 1	87.5238	66.0784	71.7842	60
Point 2	88.1583	64.8706	71.4295	60
Point 3	90.0115	64.8283	72.526	60
Point 4	90.2549	64.9456	72.0448	60
Point 5	89.938	65.0005	72.0231	60
Point 6	84.7433	60.127	69.997	60
Point 7	87.0809	60.0015	71.1047	60
Point 8	88.1358	60.2381	71.3403	60
Point 9	88.3389	60.3875	71.0397	60

Wafer 4: The thicknesses of the layers are very well distributed in this wafer, except for the thicker layers 3 and 5, where at some points, there is a deviation in the thicknesses of approximately 15–18 nm.

Table 4: Measured thicknesses of Wafer 4 at different points via ellipsometry.

9 Points	Layer 1 in nm	Layer 2 in nm	Layer 3 in nm	Layer 4 in nm	Layer 5 in nm	Layer 6 in nm
Point 1	87.7586	55.9182	292.041	51.8084	293.1354	50
Point 2	90.2351	54.8226	289.8662	51.438	288.685	50
Point 3	90.379	54.7569	293.5395	51.3087	293.9226	50
Point 4	90.3774	54.712	291.819	51.8251	291.7248	50
Point 5	88.6537	54.8955	291.7368	51.2499	291.9204	50
Point 6	88.3284	50.1836	282.5496	47.9144	279.096	50
Point 7	89.0099	51.2136	282.4552	45.6952	286.7646	50
Point 8	89.046	51.2511	284.7369	45.5058	289.4139	50
Point 9	86.3767	49.5665	284.7243	49.0079	281.6538	50

Wafer 5: The intended thickness for this wafer was 80 nm, which was measured via ellipsometry after fabrication at different points, and the thicknesses in Table 5 were obtained.

Table 5: Calculated thicknesses at different points of Wafer 5 via ellipsometry.

9 Points	TiN Layer in nm
Point 1	79.6944
Point 2	78.789
Point 3	78.3605
Point 4	78.7844
Point 5	78.5995
Point 6	75.6744
Point 7	73.5532
Point 8	76.2353
Point 9	73.4106

n, k for Five Wafers from Simulations in the Refit Software and Experiment

The real and imaginary parts of the refractive indices of the metals in the wafers were simulated via RefFIT software [20] and measured via ellipsometry after fabrication. Both results are more or less in good agreement with each other, with slight deviation, as shown in the plots below.

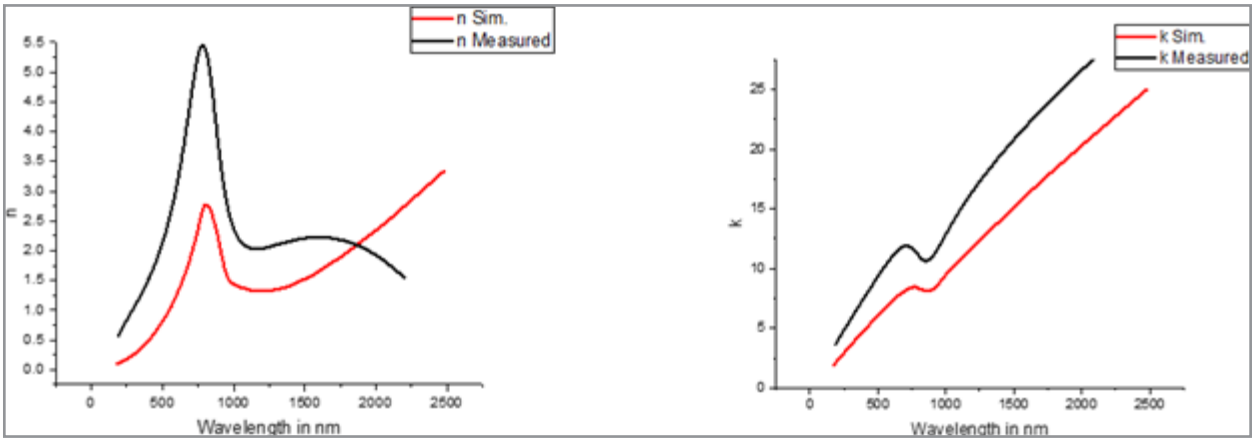

Figure 6: Comparison of n and k of Wafer 1 and Wafer 2 from simulations and ellipsometry measurements.

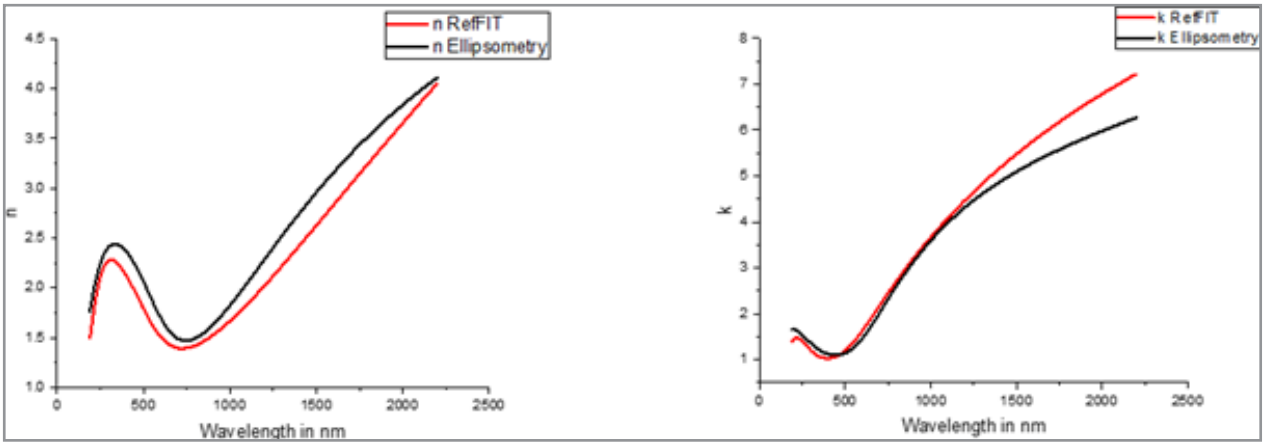

Figure 7: Comparison of n and k of Wafer 3 from simulations and ellipsometry measurements.

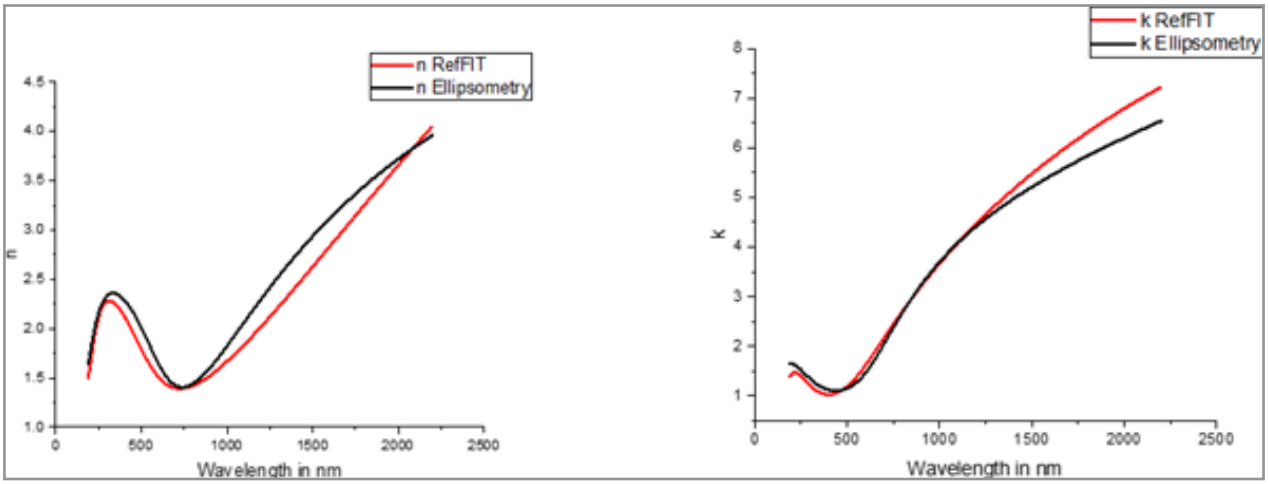

Figure 8: Comparison of n and k of Wafer 4 from simulations and ellipsometry measurements.

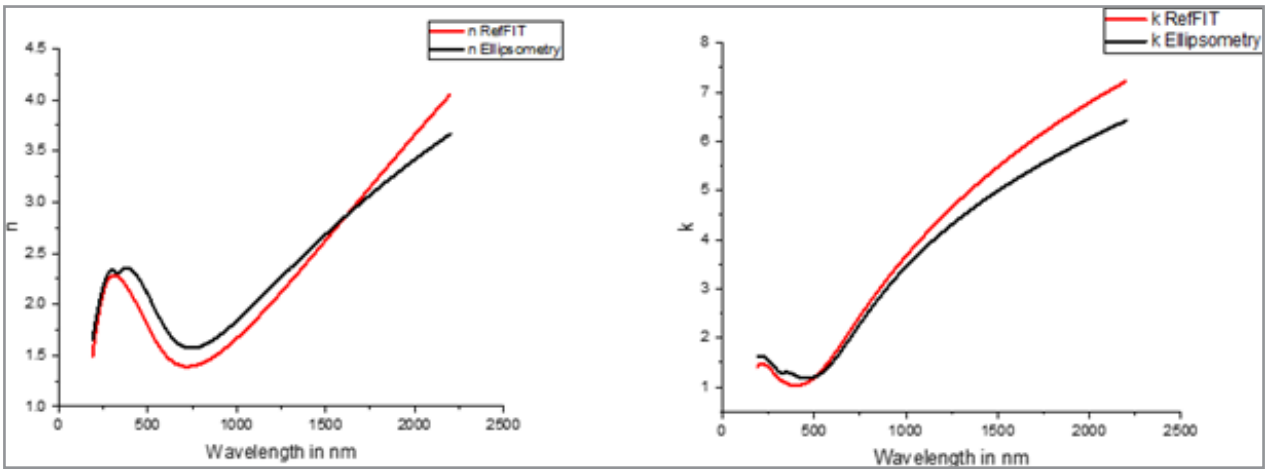

Figure 9: Comparison of n and k of Wafer 5 from simulations and ellipsometry measurements.

Tan (Psi) and Cos (Delta) from Simulations and Experiments

Tan (Psi) and Cos (Delta) give the amplitude ratio and the phase difference between the p- and s- polarized light components. Both parameters are important for studying the optical properties of thin films, providing the desired information about material composition, structure, and thickness [21] [22] [23].

Tan (Psi) indicates the ratio of the change in the amplitude of the reflected light components. This parameter is sensitive to the thickness and refractive index of the film and substrate. It is determined by the ellipsometer as the arctangent of the amplitude ratio. Cos (Delta) is related to the phase change between the p and s components. It provides information about the optical path difference and is also sensitive to the refractive index and thickness of a material. It is measured directly by an ellipsometer, typically after the phase shift is determined.

The ellipsometry parameters Psi and Delta were measured via two ellipsometers, and their values of Tan (Psi) and Cos (Delta) were calculated. These data were compared with those from the Psi and Delta obtained via simulations for the wafers in the lot. These values were measured at 59, 65 and 71 degrees between 250 nm and 900 nm for 59 degrees, between 900 nm and 2200 nm for 65 degrees, and between 250 nm and 900 nm for 71 degrees. The results are very similar and are as follows.

Wafer 1 and Wafer 2:
59 degree

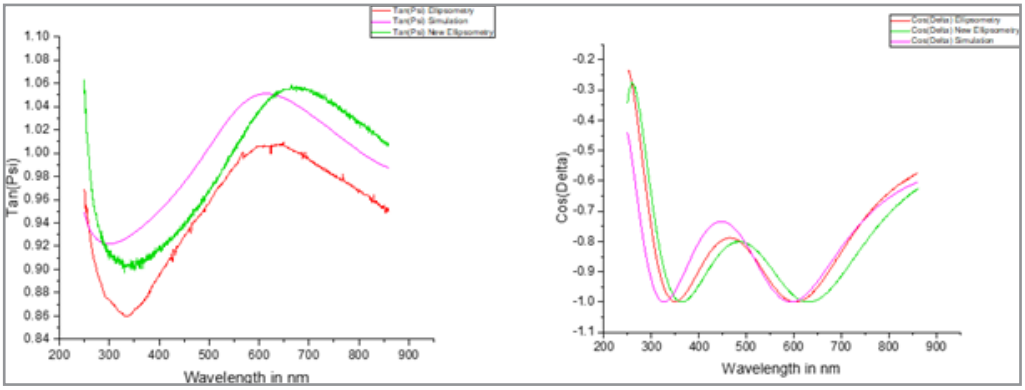

Figure 10: Calculated Tan (Psi) and Cos (Delta) of Wafer 1 and Wafer 2 from simulations and ellipsometry at a 59° angle.

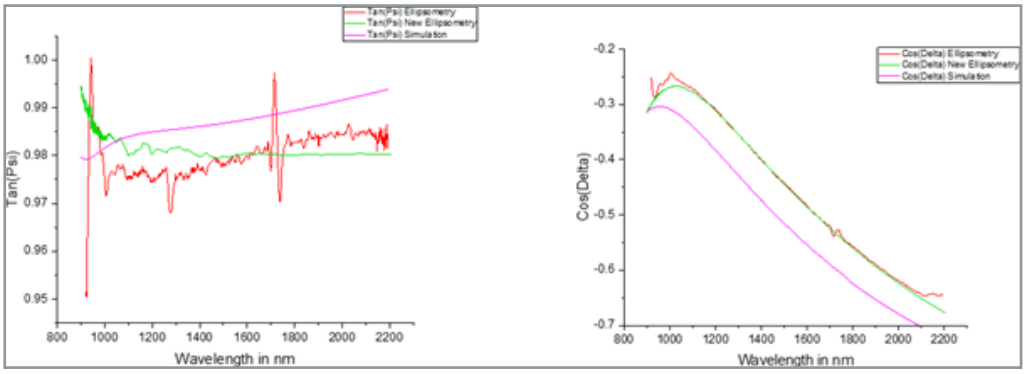

Figure 11: Calculated Tan (Psi) and Cos (Delta) of Wafer 1 and Wafer 2 from simulations and ellipsometry at a 65° angle.

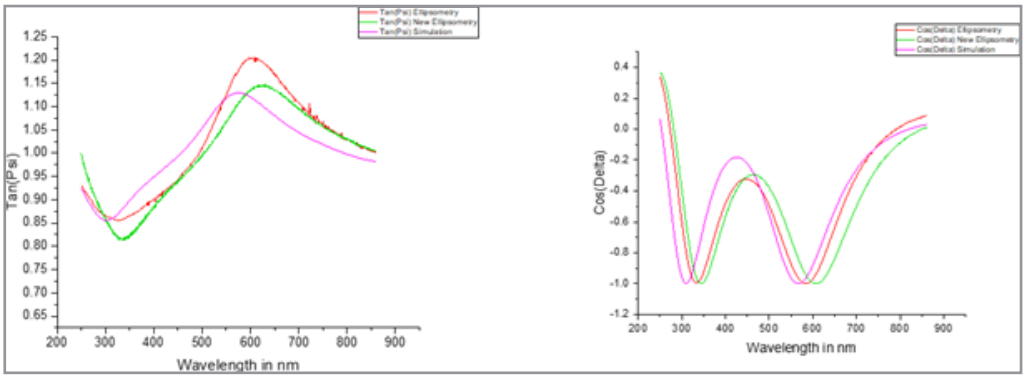

Figure 12: Calculated Tan (Psi) and Cos (Delta) of Wafer 1 and Wafer 2 from simulations and ellipsometry at a 71° angle.

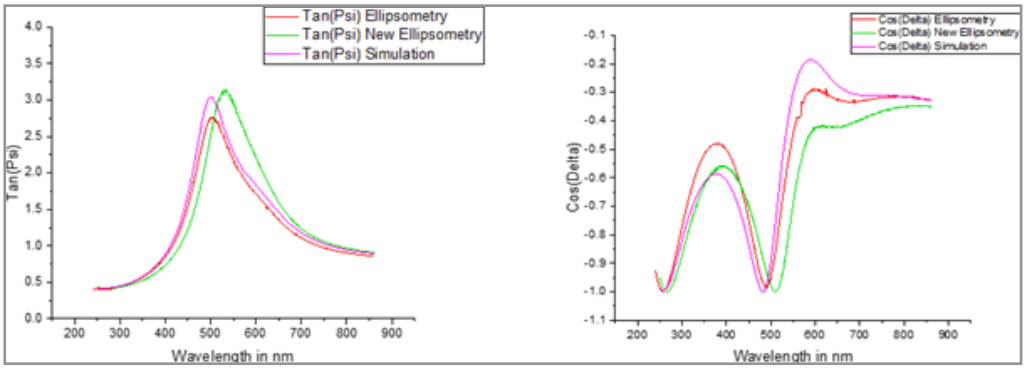

Figure 13: Calculated Tan (Psi) and Cos (Delta) of Wafer 3 from simulations and ellipsometry at a 59° angle.

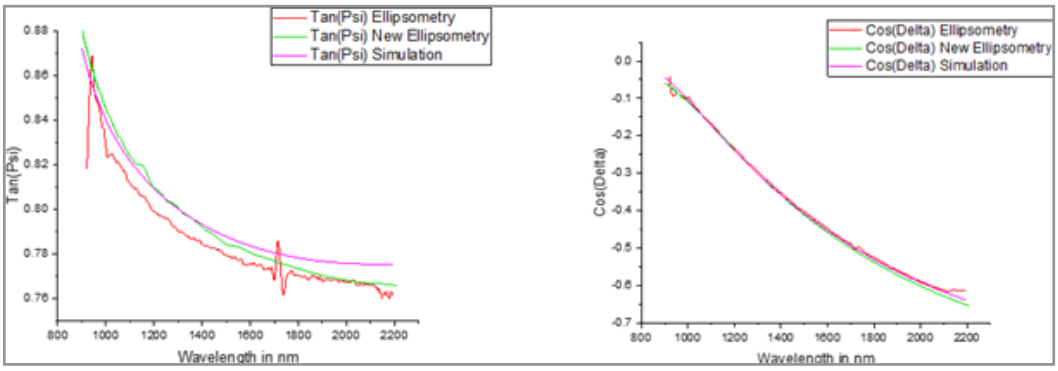

Figure 14: Calculated Tan (Psi) and Cos (Delta) of Wafer 3 from simulations and ellipsometry at a 65° angle.

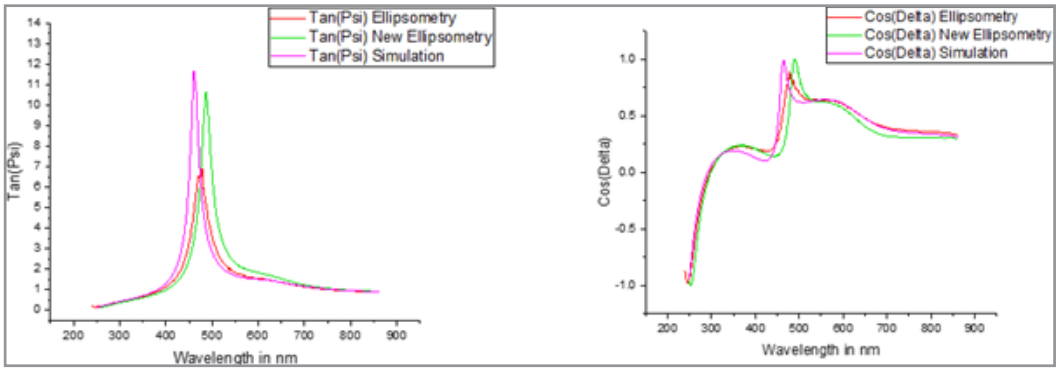

Figure 15: Calculated Tan (Psi) and Cos (Delta) of Wafer 3 from simulations and ellipsometry at a 71° angle.

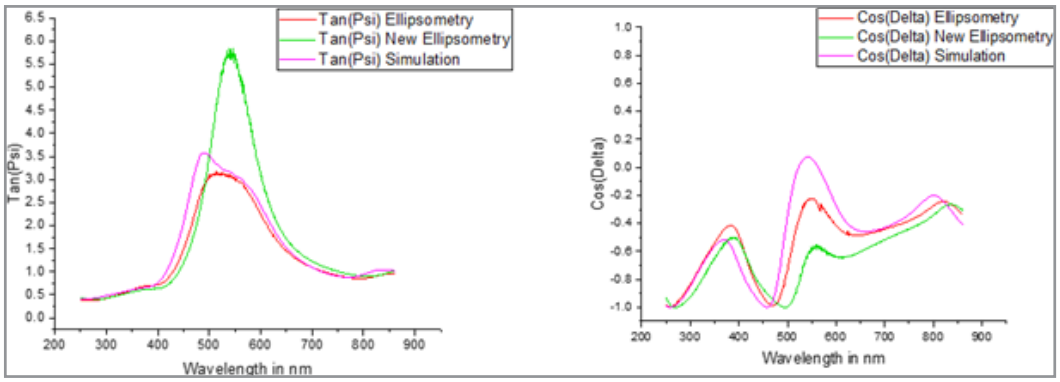

Figure 16: Calculated Tan (Psi) and Cos (Delta) of Wafer 4 from simulations and ellipsometry at a 59° angle.

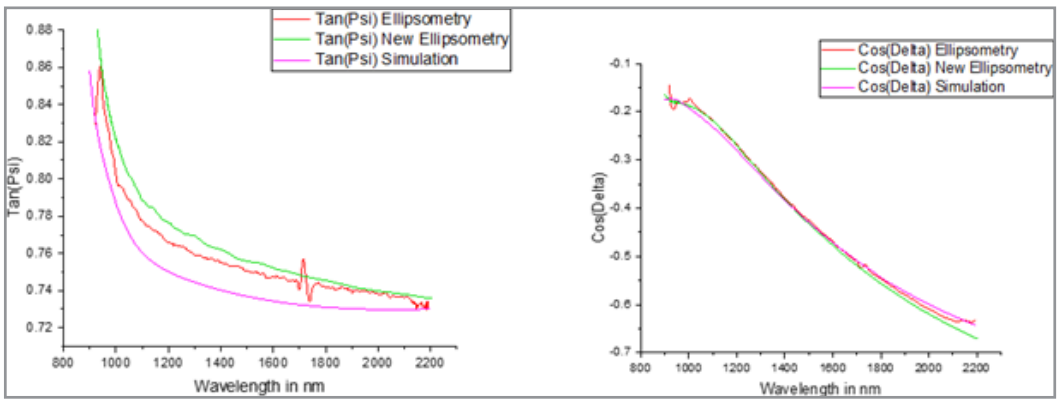

Figure 17: Calculated Tan (Psi) and Cos (Delta) of Wafer 4 from simulations and ellipsometry at a 65° angle.

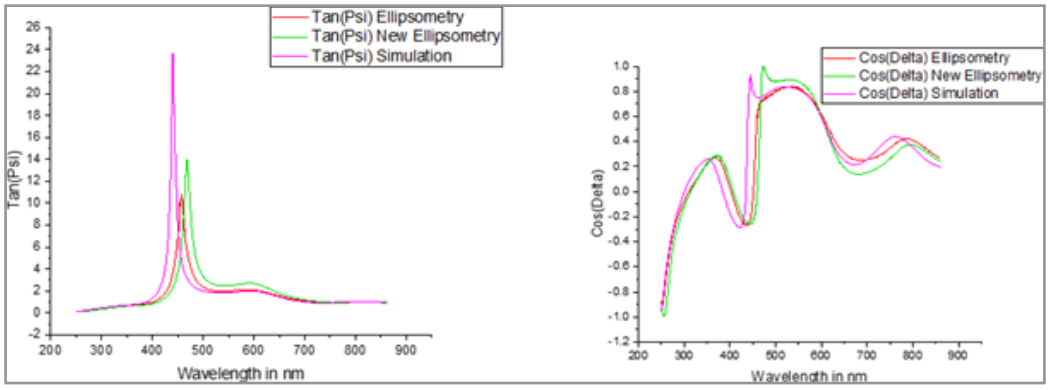

Figure 18: Calculated Tan (Psi) and Cos (Delta) of Wafer 4 from simulations and ellipsometry at a 71° angle.

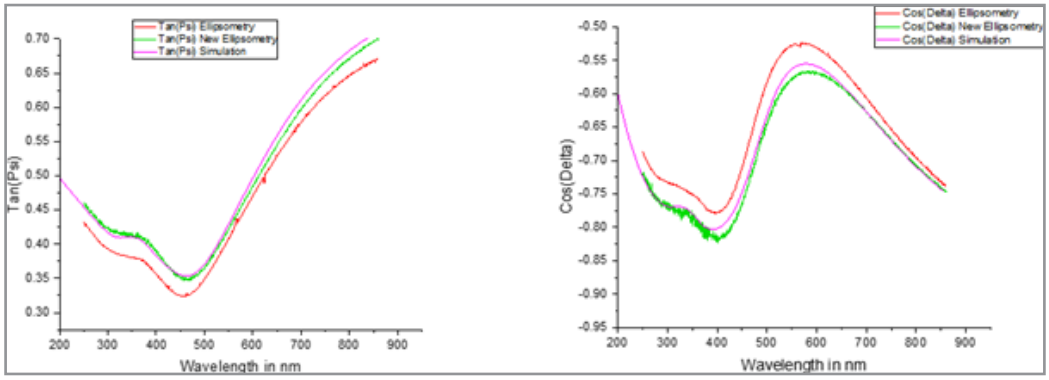

Figure 19: Calculated Tan (Psi) and Cos (Delta) of Wafer 5 from simulations and ellipsometry at a 59° angle.

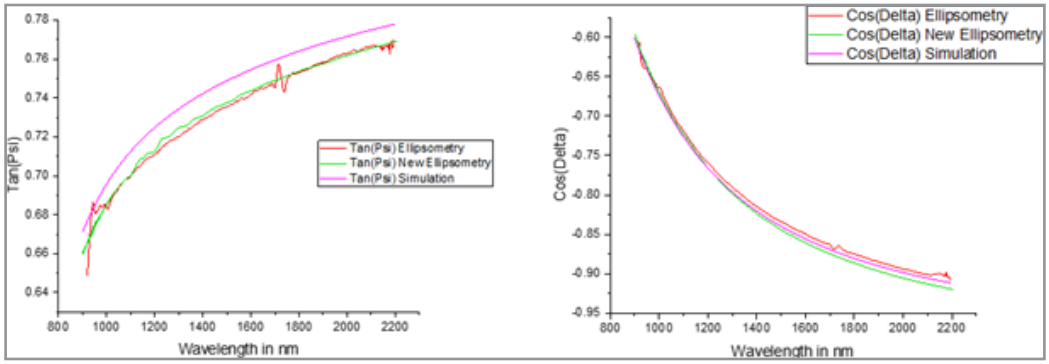

Figure 20: Calculated Tan (Psi) and Cos (Delta) of Wafer 5 from simulations and ellipsometry at a 65° angle.

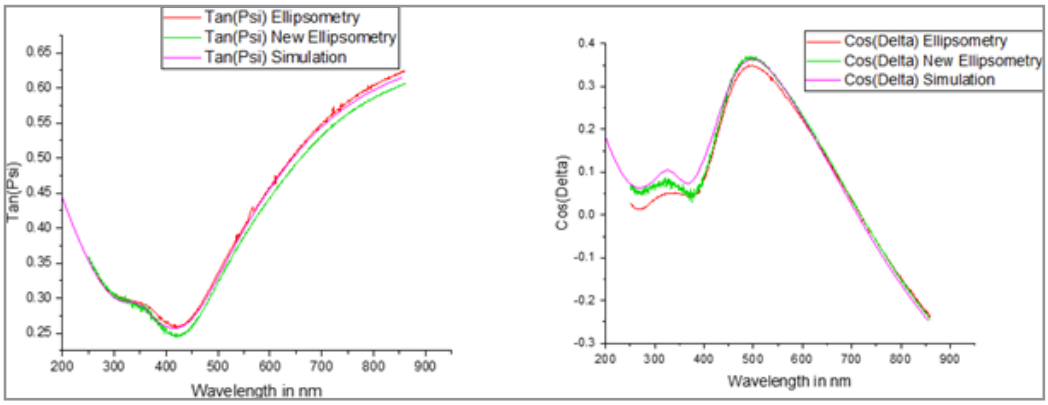

Figure 21: Calculated Tan (Psi) and Cos (Delta) of Wafer 5 from simulations and ellipsometry at a 71° angle.

Conclusion

Five multilayer wafers were designed and studied via TMM simulations, and the relevant optical properties of the fabricated wafers were measured or calculated via two ellipsometers and a scanning electron microscope. The data from the simulations and ellipsometry were consistent with each other, with little difference owing to the small variation in the thicknesses of the fabricated wafers. The thicknesses, refractive indices and ellipsometry parameters of the fabricated wafers were measured and compared with those of the simulations. The thicknesses of the fabricated wafers were determined by scanning electron microscopy images and one of the two ellipsometers. There was little variation in the thickness of each multilayer with respect to the designed multilayer. This is common for the fabrication techniques used for these wafers. The variations were negligible.

In Wafers 1–4, the top MIM part of the multilayers, for example, forms a Fabry–Perot cavity, which is used to create a resonance in the absorption spectrum of the wafer; hence, they can be designed and modified to peak at the desired wavelength. The absorption spectra of Wafer 1 and Wafer 2 were identical, with a well-defined peak around the bandgap wavelength of GaAs (870 nm), because their top Fabry–Perot cavities were made of the same metal with the same thickness. Almost all of the absorption takes place in this top Fabry–Perot cavity and hence has the same absorption spectrum, with the same intensity and wavelengths of the absorption peaks.

Much greater absorption was observed for Wafer 3 and Wafer 4, which were made with alternating TiN/silica multilayers. The absorption spectra obtained via TMM simulations for these two wafers were studied to determine whether they are good for use as selective emitters for a TPV system, but a sudden drop in the intensity is not observed, as would be required in the case of a good selective emitter. Therefore, these parameters were used to study other parameters of multilayers, such as the refractive index, thickness after fabrication, ellipsometry parameters, etc.

Wafer 5 was a very thin TiN layer on a silicon substrate meant to be a test wafer. The desired thickness of the fabricated wafer was instructed to be between 50 nm and 100 nm, and the thickness of this TiN layer was determined via ellipsometry to be approximately 80 nm. The thicknesses of all the fabricated wafers were measured at 9 different points across each wafer, and the thicknesses were almost the same at all 9 points. This confirmed that the thickness of the layers is more or less uniform across the wafer and thus is a positive outcome of the fabrication methods.

The dependence of n and k on the wavelength for all the designed wafers was simulated via RefFIT software and compared with those of the fabricated wafers via one of the two ellipsometers, and the results were in good agreement. The ellipsometry parameters Psi and Delta were measured via two ellipsometers, and their values of Tan (Psi) and Cos (Delta) were calculated. These data were compared with the data obtained via simulations for all the wafers in the lot. These parameters were measured at different angles of incidence and different wavelength ranges. The results were very similar. In conclusion, the results of this paper strongly root for the design of multilayer stacks using TMM for many applications.

Reference

1. Angus, M. H. (2010). Thin-film optical filters. https://kashanu.ac.ir/Files/thin%20film%20optical%20filter(macklod).pdf
2. Green, M. A., Emery, K., Hishikawa, Y., Warta, W. (2011). Solar cell efficiency tables (version 37). Progress in Photovoltaics: Research and Applications, 19(1), 84-92.
3. Venkata Subramanian, R., Sevilla, E., Colpitts, T., O'Quinn, B. (2001). Thin-film thermoelectric devices with high room-temperature figures of merit. Nature, 413(6856), 597-602.
4. Heavens, O. S. (1991). Optical properties of thin solid films. Dover Publications. https://archive.org/details/opticalpropertie0000heav
5. Ohring, M. (2002). Materials science of thin films: Deposition and structure (2nd ed.). Academic Press. https://www.sciencedirect.com/book/9780125249751/materials-science-of-thin-films
6. Smith, D. L. (1995). Thin-film deposition: Principles and practice. McGraw-Hill. https://archive.org/details/thinfilmdepositi0000smit
7. Morosanu, C. (1990). Thin films by chemical vapour deposition. Elsevier. https://www.sciencedirect.com/book/9780444988010/thin-films-by-chemical-vapour-deposition
8. Seshan, K. (2012). Handbook of thin film deposition (3rd ed.). William Andrew Publishing. https://www.sciencedirect.com/book/9781437778731/handbook-of-thin-film-deposition
9. Ohring, M. (2002). Materials science of thin films: Deposition and structure (2nd ed.). Academic Press. https://www.sciencedirect.com/book/9780125249751/materials-science-of-thin-films
10. Harper, J. M. E. (1982). Sputtering onto semiconductor surfaces. Journal of Vacuum Science & Technology, 20(3), 699-705.
11. Wei, D. (2010). Introduction to sputtering and thin film technology. Cambridge University Press. https://assets.cambridge.org/97805216/24602/frontmatter/9780521624602_frontmatter.pdf
12. Green, M. A., Emery, K., Hishikawa, Y., Warta, W. (2013). Solar cell efficiency tables (version 42). Progress in Photovoltaics: Research and Applications, 21(5), 827-837.
13. Campbell, S. A. (2008). The science and engineering of microelectronic fabrication (2nd ed.). Oxford University Press. http://dei-s1.dei.uminho.pt/outraslic/lebiom/micro_1/download/Microelectronics_Fabrication.pdf
14. Chang, C. Y., Sze, S. M. (1996). ULSI technology. McGraw-Hill. https://archive.org/details/ulsitechnology0000unse
15. Wolf, S., Tauber, R. N. (2000). Silicon processing for the VLSI era: Volume 1: Process technology. Lattice Press. https://www.amazon.in/Silicon-Processing-Vlsi-Era-Technology/dp/0961672137
16. Datas, A., Martí, A. (2017). Thermophotovoltaic energy in space applications: Review and future potential. Solar Energy Materials and Solar Cells, 161, 285-296.
17. Ngan, P. S., Cheung, H. K. (2005). Selective emitters for thermophotovoltaic applications. Journal of Applied Physics, 98(1), 014912.

18. Coutts, T. J., Fitzgerald, M., Gee, J. M. (1998). Thermophotovoltaics: The state of the art. Journal of Vacuum Science & Technology A: Vacuum, Surfaces, and Films, 16(2), 948-961.
19. Yariv, A., Yeh, P. (2007). Photonics: Optical electronics in modern communications (6th ed.). Oxford University Press. https://authors.library.caltech.edu/records/z5c1t-ddk31
20. Kuzmenko, A. B. (2005). Kramers–Kronig constrained variational analysis of optical spectra. Review of Scientific Instruments, 76, 083108.
21. Azzam, R. M. A., Bashara, N. M. (1987). Ellipsometry and polarized light (2nd ed.). North Holland. https://www.amazon.com/Ellipsometry-Polarized-North-Holland-Personal-Library/dp/0444870164
22. Fujiwara, H. (2007). Spectroscopic ellipsometry: Principles and applications. John Wiley & Sons. https://onlinelibrary.wiley.com/doi/book/10.1002/978047006019
23. Tompkins, H. G., Irene, E. A. (2005). Handbook of ellipsometry. William Andrew Publishing. https://dl.icdst.org/pdfs/files/292d75c8c2e53fe664af5daffaa461cb.pdf